GlueX-doc-856-v1
Updated: November 19, 2007

GlueX Calorimetry - An Overview

Alex R. Dzierba
Department of Physics
Indiana University, Bloomington, IN 47405

Abstract

This is a draft of the introductory and summary sections of the Calorimetry chapter of the GlueX Detector Design Report.

1 Introduction

To achieve the primary physics goal of GlueX, *i.e.* mapping out the spectrum of gluonic excitations, it is essential to detect photons with good acceptance and to measure their energies, positions and arrival times with sufficient resolution. The photons of particular interest are those resulting from $\pi^0 \to \gamma\gamma$ and $\eta \to \gamma\gamma$ decays. The requirements on acceptance and on energy, position and timing resolution are driven by the need to identify exclusive reactions in order to perform the amplitude analyses that will extract meson J^{PC} quantum numbers and on the need to be sensitive to a variety of meson decay modes.

There is little data on meson photoproduction in the GlueX energy regime ($E_\gamma \approx 7 - 9$ GeV). Almost all of what is known comes from bubble chamber measurements at SLAC [1, 2, 3, 4, 5, 6]. These experiments were among the first exploratory studies of the photoproduction of mesons and baryon at these energies, and although they suffer from low-statistics, these bubble chamber experiments have good acceptance, except for events with multiple neutrals. Exclusive reactions leading to final states with charged particles and a single neutron or π^0 can be identified by kinematic fitting. Table 1 summarizes the photoproduction cross sections for various charged particle topologies, with and without neutrals, at $E_\gamma = 9.3$ GeV [1]. Final states with single or multi-neutral particles (π^0, η or n) account for about 82% of the total cross section. About 13% of the total cross section is due to final states with charged particles and a single π^0. So for about 70% of the total photoproduction cross section, from $E_\gamma \approx 7$ to ≈ 12 GeV, we have essentially no information. Extrapolating from what is known from the final states that have been identified and studied, the bulk of the unknown processes are expected to involve final states with combinations of π^0 and η mesons. The discovery potential of GlueX rests on being able to detect π^0 and η mesons.

Topology	σ (μb)	% of σ with neutrals
1-prong	8.5 ± 1.1	100
3-prong	64.1 ± 1.5	76 ± 3
5-prong	34.2 ± 0.9	86 ± 4
7-prong	6.8 ± 0.3	86 ± 6
9-prong	0.61 ± 0.08	87 ± 21
With visible strange decay	9.8 ± 0.4	-
Total	124.0 ± 2.5	82 ± 4

Table 1: Topological photoproduction cross sections for γp interactions at 9.3 GeV from Reference [1]. Also shown are the percent of the cross section with neutral particles for each topology.

1.1 Decay modes of exotic hybrid mesons

Table 2 lists several J^{PC} exotic mesons and their favored decay modes. For example, according to the flux tube model and lattice QCD, the preferred decay modes for exotic hybrids are into $(q\bar{q})_P + (q\bar{q})_S$ mesons such as $b_1 + \pi$ or $f_1 + \pi$. Table 3 lists candidate exotic $J^{PC} = 1^{-+}$ state for which evidence has been claimed. The purported exotic states include decay modes into $b_1\pi$ or $f_1\pi$ as well as decay modes into $\eta\pi$ and $\eta'\pi$. The decays into two pseudoscalars are attractive in their simplicity since the charge conjugation quantum number C is required to be positive, the spin of this two spinless meson system is $J = L$ where L is the relative angular momentum between the mesons and parity is given by $P = (-1)^L$. Thus, identifying a P-wave decay leads to manifestly exotic quantum numbers. The dominant branching fractions for meson states listed among the decay products are summarized in Table 4. Clearly, exotic meson spectroscopy requires the ability to detect and measure the π^0 and η mesons.

Some of the preferred or observed exotic hybrid decay modes listed in Tables 2 and 3 do not necessarily involve π^0 mesons, *e.g.* the $\rho\pi$ or $a_2\pi$ modes – these can have final states that only involve $\pi^\pm$ such as $(\rho\pi)^+ \to \pi^+\pi^+\pi^-$. But if a state decays into such an all charged π system, having the isospin partners available, such as $(\rho\pi)^+ \to \pi^+\pi^0\pi^0$ provides important isospin consistency checks of the amplitude analysis and understanding of the detector acceptance.

Exotic Meson	J^{PC}	I	G	Possible Modes
b_0	0^{+-}	1	+	
h_0	0^{+-}	0	−	$b_1\pi$
π_1	1^{-+}	1	−	$\rho\pi$, $b_1\pi$
η_1	1^{-+}	0	+	$a_2\pi$
b_2	2^{+-}	1	+	$a_2\pi$
h_2	2^{+-}	0	−	$\rho\pi$, $b_1\pi$

Table 2: Predicted J^{PC} exotic hybrid mesons and their expected decay modes. See Table 4 for decay modes of the b_1 and a_2 mesons.

Exotic Meson Candidate	Decay Mode
$\pi_1(1400)$	$\pi^-\eta$
	$\pi^0\eta$
$\pi_1(1600)$	$\rho^0\pi^-$
	$\eta'\pi^-$
	$b_1\pi$
	$f_1\pi$

Table 3: Reported $J^{PC} = 1^{-+}$ exotic hybrid mesons and their decay modes. See Table 4 for decay modes of the η', b_1 and f_1 mesons. Source: 2006 Review of Particle Physics [7].

1.2 Baryon resonance decays involving π^0

Photoproduction of meson resonances in the GlueX energy regime typically result in the produced meson being produced at small absolute values of the momentum transfer squared $|t|$ between incoming photon and outgoing meson – or equivalently between target proton and recoil nucleon or baryon resonance. The produced meson, as well as its decay products (depending on the particle multiplicity and relative mother-daughter masses), move in the forward direction whereas the recoil baryon moves at large angles $\gtrsim 45^\circ$ with respect to the beam direction. If the recoil baryon is a baryon resonance, such as a Δ or N^*, decays involving π^0 are possible. It will important to identify the soft, wide-angle π^0 mesons from such decays since the amplitude analysis depends on starting with a known exclusive reaction.

2 π^0 and η Kinematics

2.1 Overview

Here we review how the decay photons from photoproduced meson and baryon resonances populate LAB energy-angle space at GlueX energies. In order to put this into context, please refer to Figure 1 which

Meson Decay Mode	Branching Fraction (%)
$\pi^0 \to 2\gamma$	99
$\eta \to 2\gamma$	39
$\eta \to 3\pi^0$	33
$\eta \to \pi^+\pi^-\pi^0$	23
$\omega \to \pi^+\pi^-\pi^0$	89
$\omega \to \pi^0\gamma$	9
$\eta' \to \pi^+\pi^-\eta$	45
$\eta' \to \pi^0\pi^0\eta$	21
$\eta' \to 2\gamma$	2
$b_1(1235) \to \omega\pi$	dominant
$f_1(1285) \to \pi^0\pi^0\pi^+\pi^-$	22
$f_1(1285) \to \eta\pi\pi$	52
$a_2(1320) \to 3\pi$	70
$a_2(1320) \to \eta\pi$	15

Table 4: Neutral or charged + neutral decay modes of several well established mesons. Source: 2006 Review of Particle Physics [7].

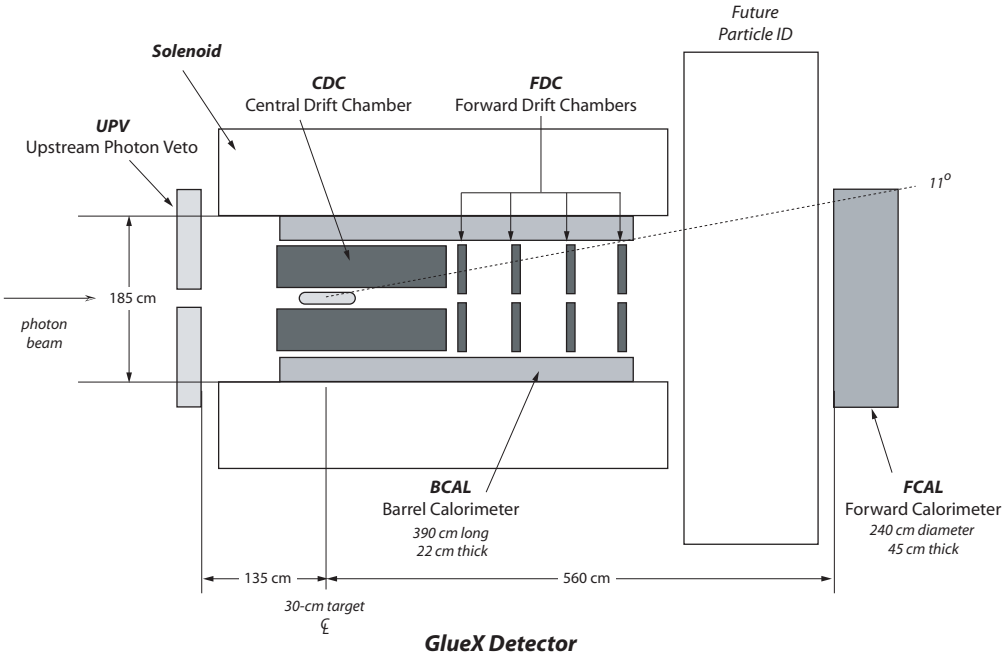

Figure 1: Schematic of the GlueX Detector. Electromagnetic calorimeter elements are shown in light gray and tracking elements in dark gray. The detector is cylindrically symmetric about the beam line. The dotted line from the target center to the edge of downstream plane of FCAL indicates is at 11° – for larger photon angles, BCAL is used to measure energy and position, while for smaller angles, FCAL is used to provide the measurements.

shows a schematic of the GlueX detector. The detector has cylindrical symmetry about the beam axis. The dimensions and placement of the critical charged particle tracking elements inside the 2 T solenoidal magnetic field volume are shown. These tracking elements are discussed elsewhere in more detail, but their number and placement are driven by the desire to provide momentum resolution of sufficient accuracy. The

tracking system consist of cylindrical straw tube drift chamber (CDC) surrounding the target and four planar drift chamber packages comprising the forward drift chambers (FDC). The electromagnetic calorimeters for photon measurements consist of a cylindrical, barrel-shaped calorimeter (BCAL) and a forward calorimeter (FCAL). The dotted line from the target center to the edge of downstream plane of FCAL indicates is at 11° – for larger photon angles, BCAL is used to measure energy and position, while for smaller angles, FCAL is used to provide the measurements.

2.2 Studies using Pythia

As noted above, much is unknown about photoproduction at GlueX energies leading to multi-neutral final states. To estimate photon yields we used the Monte Carlo program Pythia [8] that was written to generate high energy physics events produced in a wide variety of initial states, including fixed target photoproduction. The program is based on a combination of analytical results and QCD-based models of particle interactions Pythia was designed to allow for tuning parameters to suit the particular situation and it has been tuned for photoproduction at 9 GeV. The output of the simulations were compared [9] to published data, in particular, reference [1]. Comparison of cross section estimates for charged particle topologies and several reactions in the 3-prong and 5-prong, which accounts for 80% of the total cross section, are shown in Tables 5 and 6. The vector mesons ρ, ω and ϕ appear in the 3-prong sample in the $\pi^+\pi^-p$, $\pi^+\pi^-\pi^0p$ and K^+K^-p final states respectively. The distribution in $|t|$ for Pythia events agree with published data for specific reactions. Pythia accounts for Δ resonance production. In the $\pi^+\pi^-K^+K^-p$ state, the $K^*(890)$ is present.

Topology	Pythia Estimates (μb)	Data (μb)
1-prong	8.8 ± 0.02	8.5 ± 1.1
3-prong	63.5 ± 0.09	64.1 ± 1.5
5-prong	42.7 ± 0.2	34.2 ± 0.9
7-prong	7.3 ± 0.1	6.8 ± 0.3
9-prong	0.3 ± 0.1	0.61 ± 0.08

Table 5: Topological Photoproduction Cross Sections at 9 GeV from Pythia and from bubble chamber data [1]. The Pythia cross section estimates assume a total photoproduction cross section of 124 μb. The errors on the Pythia estimates are statistical.

Figure 2 shows the photon multiplicity for 1M Pythia events with vertices generated uniformly over the length of the 30-cm, as shown in Figure 1. About 78% of the events have at least on photon leading to a total of 3.8M photons, of which 27.8% enter FACL, 70.5% enter BCAL and 1.7% enter UPV. The correlation of photon energy with angle for all photons, FCAL photons, BCAL photons and UPV photons is also shown in Figure 2.

Reaction	Pythia Estimates (μb)	Data (μb)
	$\gamma p \to 3$ prongs	
$\gamma p \to p\pi^+\pi^-$	13.6 ± 0.13	14.7 ± 0.6
$\gamma p \to pK^+K^-$	0.41 ± 0.02	0.58 ± 0.05
$\gamma p \to p\bar{p}p$	0.04 ± 0.01	0.09 ± 0.02
$\gamma p \to p\pi^+\pi^-\pi^0$	5.8 ± 0.1	7.5 ± 0.8
$\gamma p \to n2\pi^+\pi^-$	1.4 ± 0.04	3.2 ± 0.7
With multi-neutrals	42.3 ± 0.3	38.0 ± 1.9
	$\gamma p \to 5$ prongs	
$\gamma p \to p2\pi^+2\pi^-$	2.9 ± 0.06	4.1 ± 0.2
$\gamma p \to pK^+K^-\pi^+\pi^-$	0.51 ± 0.03	0.46 ± 0.08
$\gamma p \to p2\pi^+2\pi^-\pi^0$	8.12 ± 0.1	6.7 ± 1.0
$\gamma p \to n3\pi^+2\pi^-$	$0.8 \pm .3$	1.8 ± 1.9
With multi-neutrals	30.4 ± 0.2	21.1 ± 1.7

Table 6: Photoproduction reaction cross sections at 9 GeV from Pythia and from bubble chamber data [1]. The Pythia cross section estimates assume a total photoproduction cross section of 124 μb. The errors on the Pythia estimates are statistical.

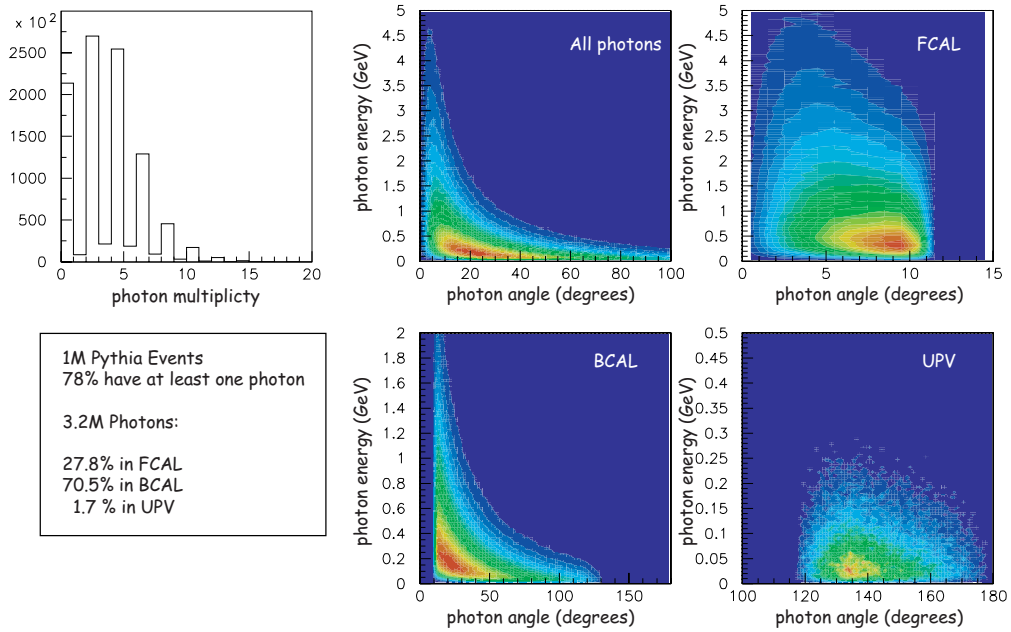

Figure 2: Left: Photon multiplicity for 1M Pythia events with vertices generated uniformly over the length of the 30-cm as shown in Figure 1. About 78% of the events have at least on photon leading to 3.8M photons, of which 27.8% enter FACL, 70.5% enter BCAL and 1.7% enter UPV. Right: Correlation of photon energy and angle for all photons, FCAL photons, BCAL photons and UPV photons.

References

[1] H. H. Bingham et al. Total and partial γp cross sections at 9.3 GeV. *Phys. Rev.*, D8:1277–1286, 1973.

[2] J. Ballam et al. Vector meson production by polarized photons at 2.8, 4.7 and 9.3 GeV. *Phys. Rev.*, D7:3150–3177, 1973.

[3] Y. Eisenberg et al. Photoproduction of ω mesons from 1.2 to 8.2 GeV. *Phys. Lett.*, B34:439–442, 1971.

[4] Y. Eisenberg et al. Study of high energy photoproduction with positron-annihilation radiation. I. Three-prong events. *Phys. Rev.*, D5:15–38, 1972.

[5] G. Alexander et al. Study of high energy photoproduction with positron-annihilation radiation. II. The reaction $\gamma p \to p\pi^+\pi^+\pi^-\pi^-$. *Phys. Rev.*, D8:1965–1978, 1973.

[6] G. Alexander et al. Study of high energy photoproduction with positron-annihilation radiation. III. The reactions $\gamma p \to p2\pi^+2\pi^-\pi^0$ and $\gamma p \to n3\pi^+2\pi^-$. *Phys. Rev.*, D9:644–648, 1974.

[7] W.-M. Yao et al. Review of particle physics. *J. Phys.*, G33:1, 2006.

[8] T. Sjöstrand, S. Mrenna, and P. Skands. Pythia 6.4 Physics and Manual. Technical report, Lund University, 2006. hep-ph/0603175 and http://www.thep.lu.se/~torbjorn/Pythia.html.

[9] A. Dzierba. Comparing Pythia Simulations with Photoproduction Data at 9 GeV. Technical report, GlueX Document, 2007. GlueX-doc-856-v1.